Long-wave infrared integrated resonators in the 7.5–9 *μ*m wavelength range ⊘

Natnicha Koompai ⓘ ; Thi Hao Nhi Nguyen ⓘ ; Victor Turpaud ⓘ ; Jacopo Frigerio ⓘ ; Virginia Falcone ⓘ ;
Stefano Calcaterra ⓘ ; Luca Lucia ⓘ ; Adel Bousseksou ⓘ ; Raffaele Colombelli ⓘ ; Jean-Rene Coudevylle ⓘ ;
David Bouville; Carlos Alonso-Ramos ⓘ ; Laurent Vivien; Giovanni Isella ⓘ ; Delphine Marris-Morini ✉ ⓘ

Check for updates

View
Online

Export
Citation

CrossMark

Articles You May Be Interested In

Mid-infrared integrated silicon–germanium ring resonator with high Q-factor

APL Photonics (July 2023)

Theoretical investigation of a low-voltage Ge/SiGe multiple quantum wells optical modulator operating at
1310 nm integrated with Si_3N_4 waveguides

AIP Advances (November 2018)

UAV mission planning interface development with trajectory optimization algorithm

AIP Conference Proceedings (July 2019)

AIP
Publishing
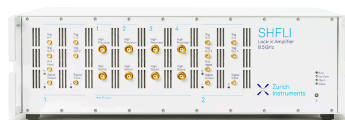
Long-wave infrared integrated resonators in the 7.5–9 µm wavelength range

View Online   Export Citation   CrossMark

Natnicha Koompai,[1] Thi Hao Nhi Nguyen,[1] Victor Turpaud,[1] Jacopo Frigerio,[2] Virginia Falcone,[2]
Stefano Calcaterra,[2] Luca Lucia,[1] Adel Bousseksou,[1] Raffaele Colombelli,[1] Jean-Rene Coudevylle,[1]
David Bouville,[1] Carlos Alonso-Ramos,[1] Laurent Vivien,[1] Giovanni Isella,[2] and Delphine Marris-Morini[1,a]

AFFILIATIONS

[1]Centre de Nanosciences et de Nanotechnologies, Université Paris-Saclay, CNRS, 91120 Palaiseau, France
[2]L-NESS, Dipartimento di Fisica, Politecnico di Milano, Polo di Como, Via Anzani 42, 22100 Como, Italy

[a]Author to whom correspondence should be addressed: delphine.morini@universite-paris-saclay.fr

ABSTRACT

We present broadband on-chip resonators based on SiGe graded-index waveguides operating in the long-wave infrared spectral range from 7.5 to 9.0 µm wavelength range. A quality factor up to 10^5 has been measured, while an intrinsic quality factor of 1.13×10^5 has been extracted from the measurements. Thermal tuning of the phase in the micro-ring has been used to overcome the limitation of the experimental setup in terms of spectral resolution. These results pave the way toward the development of integrated frequency comb operating in the long-wave infrared range.

Published under an exclusive license by AIP Publishing. https://doi.org/10.1063/5.0157177

Photonic integrated circuits operating in the long-wave infrared (LWIR) spectral range have recently emerged as a highly promising technology for applications in spectroscopy and sensing because most molecules have vibrational and rotational resonances in the so-called "fingerprint" region (wavelength from 6 to 15 µm). This wavelength range can, hence, be exploited to detect small traces of environmentally hazardous and toxic substances by the analysis of the optical spectrum after its interaction with the substances to detect. A variety of applications are foreseen, including chemical sensing,[1] environmental studies,[2,3] medical diagnostics,[4] or industrial process monitoring.[5]

Among different spectroscopic techniques, dual-comb spectroscopy (DCS) is a powerful technique to measure optical spectra in a wide spectral range with a high-frequency resolution.[6] The commercialization of dual-comb spectroscopic systems based on frequency comb quantum cascade laser (QCL)[7] already shows the maturity of this technology. However, for many applications, the size, cost, and ease of use of the system are critical factors for the large-scale distribution of the systems, driving the development of compact integrated frequency comb sources. Among the different techniques to generate frequency comb on-chip, microresonator-based comb generators (also called Kerr comb) have been largely developed. Wideband frequency comb sources have been demonstrated, covering the short-wave IR (SWIR) and mid-wave IR (MWIR) spectrum, typically up to 4–5 µm wavelength.[8] However, up until now, there is no report of

microresonator-based comb generation reaching wavelengths larger than 6 µm because high-quality factor (Q-factor) integrated resonators showing simultaneously low waveguide loss, strong light confinement, and large third-order nonlinearity effect are currently missing. In this context, we tackle the realization of high Q-factor integrated resonators in the long-wave infrared (LWIR) spectral range. Several solutions are being studied to develop low-loss photonic devices in this wavelength range, including the use of III-V semiconductors[9] and chalcogenide glasses.[10] In parallel, silicon (Si) based photonics is expected to have a major impact in this field by taking benefit from the reliable and high-volume fabrication technologies already developed for microelectronic integrated circuits.[11] While classical silicon-on-insulator (SOI) waveguides face challenges for wavelengths beyond 4 µm due to the absorption of the buried SiO_2, germanium (Ge) stands as a prime candidate for the demonstration of long-wave infrared photonic integrated circuits due to its large transparency window, up to 15 µm wavelength.[12,13] Moreover, Ge is fully compatible with Si technology and shows a strong third-order nonlinearity,[14] which has already allowed the demonstration of wideband on-chip supercontinuum generation.[15,16] Ge or SiGe photonic circuits are, thus, promising candidates for the realization of on-chip frequency combs, provided that high Q-factor resonators can be implemented. While many integrated resonators have been reported at wavelengths below 6 µm,[17,18] there have been only a few reports beyond 6 µm wavelength: (i) Ge-on-Si

resonators have reached 11 μm wavelength with a Q-factor of 10^4,[19] (ii) Ge microdisks coupled with partially suspended waveguide on a separated circuit allowed the demonstration of a Q-factor of 2.5×10^5 at 8 μm wavelength,[20] and (iii) broadband-integrated racetrack ring resonators based on graded SiGe waveguides have been demonstrated with a Q-factor of 3200 around 8 μm wavelength.[21]

In this paper, we report wideband resonators operating in the 7.5–9 μm wavelength range. Considering the limitations in spectral resolution of the setups that will be detailed hereafter, thermal heaters have been implemented on the resonator to finely scan the resonance linewidths. We measured Q-factors up to 10^5 in fully integrated devices, paving the road for the implementation of microresonator-based comb generators operating in the LWIR spectral range.

One of the main challenges to develop low-loss Ge on Si waveguides is related to the difference in lattice parameter between Si and Ge. In this work, a graded SiGe epitaxial layer is, thus, used as a waveguide core, as it permits a gradual accommodation of the lattice mismatch between Si and Ge, together with good light confinement on the Ge-rich part of the waveguide, due to the refractive index increase with Ge concentration. A 6 μm-thick layer has been selected as a good compromise to achieve simultaneously low defect density for low propagation losses and good light confinement.[22] The schematic cut-view of the waveguide and the refractive index profile are shown in Figs. 1(a) and 1(b), respectively. The waveguide width and etching depth are 4 μm each. Numerical calculations in quasi-TM polarization indicate that beyond the fundamental mode, a higher order optical mode can exist in most of the wavelength range considered in the experiment (from 7.45 to 8.6 μm wavelength), while the waveguide is single mode for wavelength beyond 8.7 μm. However, it should be noted that the higher order mode is made of two lobes in the vertical direction, and not in the lateral direction as obtained more usually in optical waveguide with constant refractive index material core. We believe that this explains why this higher order mode is not excited in the photonics circuits, as can be seen from the experimental results, as there is no perturbation of light confinement in the vertical direction. The racetrack resonators are designed to operate around 8 μm.

Coupled mode theory (CMT) is used to design the coupler part. Considering a resonator radius of 250 μm and propagation losses of 1 dB/cm, a coupling coefficient around 1% is required to target a resonator Q-factor of 10^5. An example of the calculation of the symmetric coupled mode in the directional coupler and the deduced coupling coefficient (κ^2) as a function of the coupling length are reported in Figs. 1(c) and 1(d). Coupling lengths from 10 to 60 μm have been selected for the device fabrication. Furthermore, thermal heaters have been implemented to be able to fine-tune the phase in the resonator and to determine the resonance linewidth with a good resolution. They consist of a 10 μm wide metallic line located close to the waveguide, around the resonator as shown in Fig. 1(e).

In terms of fabrication, the graded-index SiGe waveguide is epitaxially grown on a Si substrate by using low-energy plasma-enhanced chemical vapor deposition (LEPECVD).[23] The device fabrication is then carried out with the first e-beam lithography to define the position of the metallic heater. 10 nm-thick titanium and 300 nm-thick gold layers are then deposited on the sample surface, followed by a lift-off process. The resonators shape is then patterned by a second e-beam lithography step and defined by inductively coupled plasma reactive ion etching (ICP-RIE) in the Fluorine chemistry. Finally, waveguide input and output facets are diced to obtain a smooth facet to couple the light from the free-space laser beam.

The schematic view of the whole setup is displayed in Fig. 2(a), along with the SEM image of the device in Fig. 2(b). In brief, laser light with vertical polarization is coupled in and out of the waveguide using ZnSe aspheric lenses (diameter is 25.4 mm and focal distance is 12 mm). Light at the output is then sent either to a sensitive mid-IR camera (to ensure that the laser is well coupled into the optical waveguide) or to a cooled Mercury Cadmium Telluride (MCT) detector connected with a lock-in detection system. All measurements of the photonic devices reported below are done in quasi-TM polarization.

First characterizations have been done with a tunable external cavity QCL (MIRCAT from Daylight solution) operating in pulsed operation (100 kHz pulse rate—5% duty cycle). In this configuration, the laser linewidth is enlarged by the pulsed operation: according to
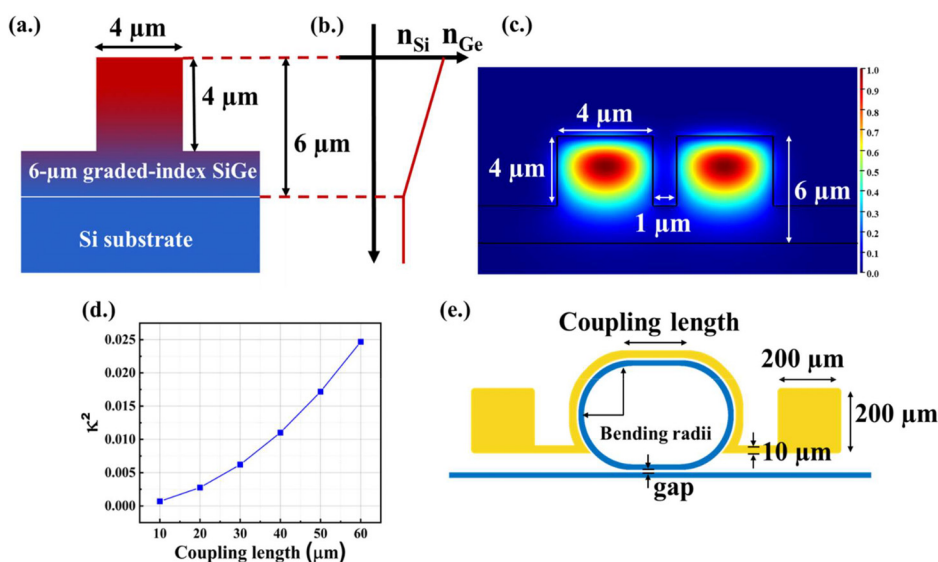
FIG. 1. (a) Schematic view of the waveguide cross section. (b) Profile of the refractive index in the SiGe layer: linear variation of the refractive index from pure Si (n = 3.42) to pure Ge (n = 4.01). (c) Symmetric coupled mode in the directional coupler for quasi-TM polarization. (d) Coupling coefficient (κ^2) as a function of the coupler length (the gap between the bus and resonator is fixed to 1 μm) at $\lambda = 8$ μm. (e) Racetrack resonator design with the implemented heater, the square heat pads of 200 μm size are used to place the DC probes.

(a.) Lock-in amplifier

Keithley source

Tunable Mid-IR Laser   Sample V_{DC} High Resolution Camera

Chopper   Aspherical Lenses   MCT Detector

(b.)

(c.)

FIG. 2. (a) Schematic view of the experimental setup. (b) SEM images of the device after fabrication of the racetrack, with zoom-in view on the directional coupler part. (c) Picture of the device during the measurement.

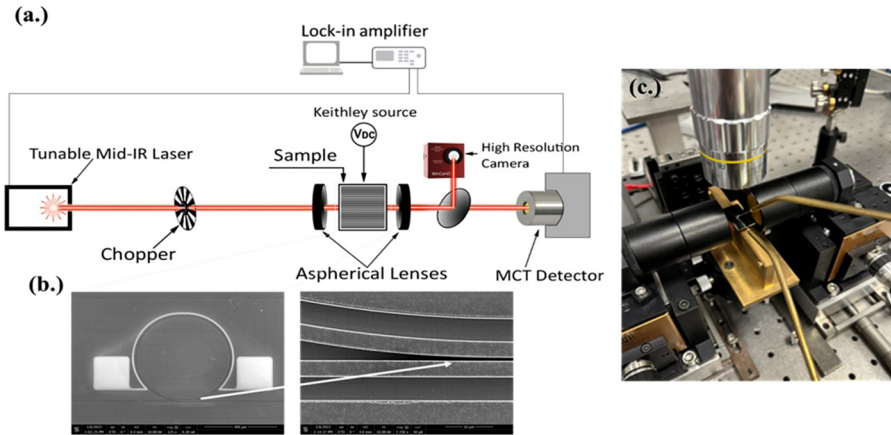the manufacturer specifications, the linewidth is around $1\,\mathrm{cm}^{-1}$ (which corresponds to 6 nm at $8\,\mu m$ wavelength), which means that the measured resonance will be smoothed by the laser linewidth. However, useful information can still be assessed from this measurement, such as the broadband operation of the devices. Examples of resonator transmission as a function of wavelength are reported in Fig. 3. The clear characteristics interferometric pattern of the resonator from 7.8 to $8.8\,\mu m$ wavelength operating in the quasi-TM polarization can be seen. Furthermore, the regular free spectral range (FSR) confirms that the light propagates only in the fundamental mode, and that there is no coupling to higher order mode in the resonator. However, in this measurement, both the resolution and extinction ratio are limited by the laser linewidth.

A broadband tunable continuous wave (CW) external cavity QCL operating from 7.45 to $9\,\mu m$ wavelength (also MIRCAT from Daylight solution) is then employed in a second experiment. While the linewidth of the laser is narrow (<100 MHz, which corresponds to 20 pm at $8\,\mu m$ wavelength), which allows, in theory, to probe cavity resonances with Q-factors up to 4×10^5, the wavelength sweep is

limited by the minimum tuning step size of $0.1\,\mathrm{cm}^{-1}$ of the laser (0.6 nm at $8\,\mu m$ wavelength), which prevents from correctly gauging the spectral width of such resonances. To circumvent this limitation, phase variation inside the resonator has been implemented to scan the resonance keeping the laser wavelength fixed. This phase variation is obtained by injecting electrical current through the integrated heater, using a current source (Keithley 2400) connected to the chip by a pair of DC probes as the schematic view of the setup in Fig. 2(a). The device under investigation with the probe set on top can be seen in Fig. 2(c). This experiment, thus, permits to measure the transmission of the resonators as a function of the electrical power dissipated in the heater. It is then important to properly estimate the variation of the phase of the light propagating in the resonator as a function of the electrical power dissipated in the heater to infer the resonance linewidth. This has been performed in different ways:

(i) Characterizations with the pulsed tunable QCL have been used to assess the heater efficiency by measuring the resonator transmitted spectra as a function of the current injected in the heater. Indeed, even if the resonance linewidth is not well resolved, it is possible to track the resonance wavelength shift as a function of the current injected in the heater and to deduce the phase shift in the resonator as a function of the electrical power dissipated in the heater. To illustrate this approach, Figs. 4(a) and 4(b) report a zoom of the transmission spectra of a racetrack resonator with a bending radius of $250\,\mu m$ with two different gaps of 0.8 and $1.0\,\mu m$, respectively, and for different values of the electrical power dissipated in the heater. First, as in Fig. 2, it can be seen that even if the resonance linewidth is not well resolved, the characteristic resonance pattern is observed, with a free spectral range (FSR) of 10.1 nm in both cases, which corresponds to a group index (n_g) of 3.8 in the resonator. The resonance shifts as a function of the electrical power dissipated in the heater are reported in Figs. 4(c) and 4(d). A resonance shift ($\Delta\lambda$) of 17.5 nm/W can be deduced from the slope of the curve. When considering dispersion effects, the variation of the effective index (Δn_{eff}) due to the thermal effect can be calculated using $\Delta n_{eff} = \Delta\lambda \times n_g/\lambda$. A value of 8.31×10^{-3}/W is obtained. Considering the thermo-optic coefficient of Ge as the thermo-optic coefficient of the
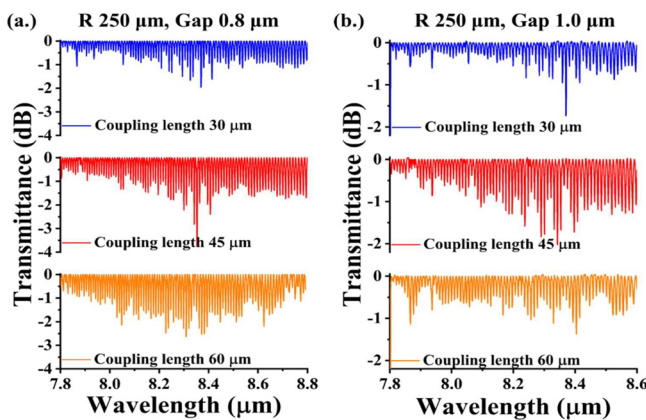

FIG. 3. Experimental transmission spectra of the racetrack resonators in quasi TM polarization with (a) gap = $0.8\,\mu m$ and (b) gap = $1.0\,\mu m$, and for different lengths of the directional coupler (30, 45, and $60\,\mu m$). Broadband operation of the resonators is observed in all cases.

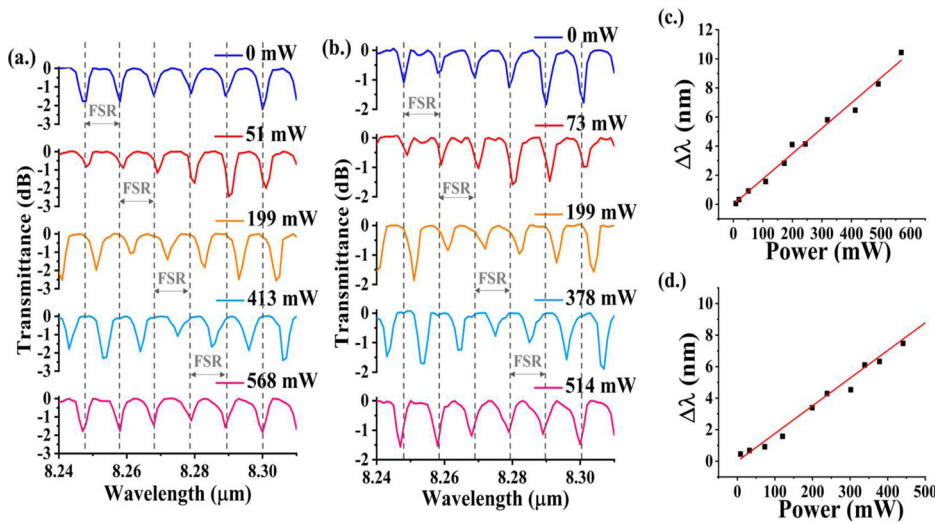**FIG. 4.** Measured transmission spectra of a racetrack resonator (radius 250 μm and coupling length 45 μm) for different power dissipated in the heater of different gaps of (a) 0.8 μm and (b) 1.0 μm; the gray lines indicate the FSR of the device. Resonance shifts around 8 μm wavelength as a function of the power dissipated in the heater of racetrack with 250 μm radius, 45 μm coupling length, and the gap of (c) 0.8 μm and (d) 1.0 μm; solid red line indicated the linear fitting used to estimate the thermal heating performance.

guided mode ($\partial n/\partial T = 4.1 \times 10^{-4}$ K^{-1}), it corresponds to an average heater efficiency of 20 K/W, which is higher than the value of 2 K/W obtained in Ref. 24 and consistent with the improvement of the heater design, especially the reduction of the distance between the optical mode center and the metallic ribbon from 12 to 8 μm.

(ii) To confirm the correct calibration procedure, the same racetracks have also been characterized in a different setup using a DFB-QCL (QD8500HHLH-Thorlabs), allowing a fine scanning of the optical spectrum but at a price of a limited spectral range (8.496–8.548 μm). Interestingly, a very good agreement has been obtained in this range, with the results obtained from the above-described calibration procedure, as can be seen in Fig. 5. The transmission of a resonator (radius 250 μm and coupling length 30 μm) is reported when measured using the DFB-QCL laser and using the CW laser and the thermal variation of the phase inside the resonator. The difference between the full width at half maximum (FWHM) measured with the two methods is less than 10%.

High-resolution measurement has, thus, been used to characterize all devices, using the CW laser at fixed wavelengths, phase variation in the resonator by tuning the current in the heater, and the method described earlier to convert the dissipated electrical power to the wavelength shift. An example of resonator transmission as a function of the wavelength is reported in Fig. 6(g). Thanks to the very good resolution (allowed by small tuning of the current in the heater), both Fabry–Pérot fringes coming from the facet of the sample and resonator resonance can be seen. The resonances appearing in the transmission spectra can be fitted with a Lorentzian function, and the full width at half maximum (FWHM) can then be extracted. The values of the FWHM are reported as a function of the wavelength for different coupling lengths of the racetrack resonator with the bending radius of 250 μm in Figs. 6(a)–6(c). The FWHM increases rapidly with the wavelength at a rate that does not stem from a variation of the coupling coefficient as a function of the wavelength. Furthermore, similar results are obtained for different values of the coupling length. Propagation losses in the resonator are, thus, expected to limit the FWHM. Losses can have different origins: waveguide losses and also

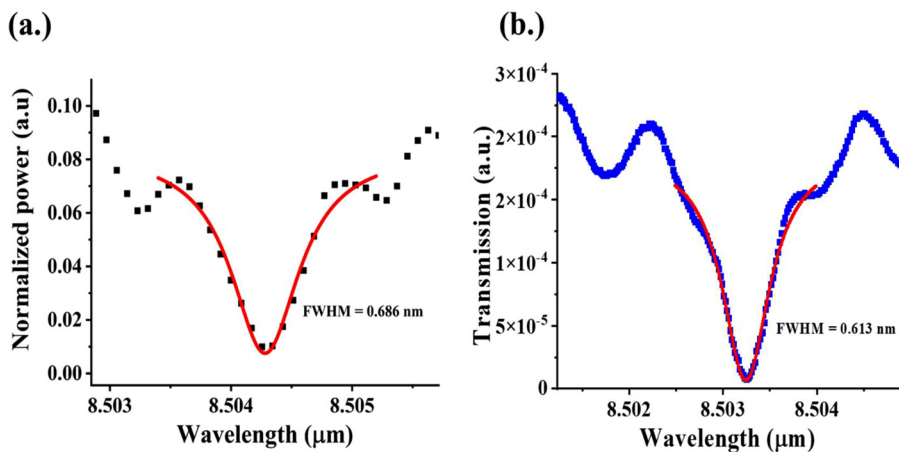

FIG. 5. Confirmation of the calibration procedure. Transmission of a resonator (radius 250 μm and coupling length 30 μm) when measured (a) using the DFB-QCL laser and (b) using the CW laser and thermal variation inside the resonator.
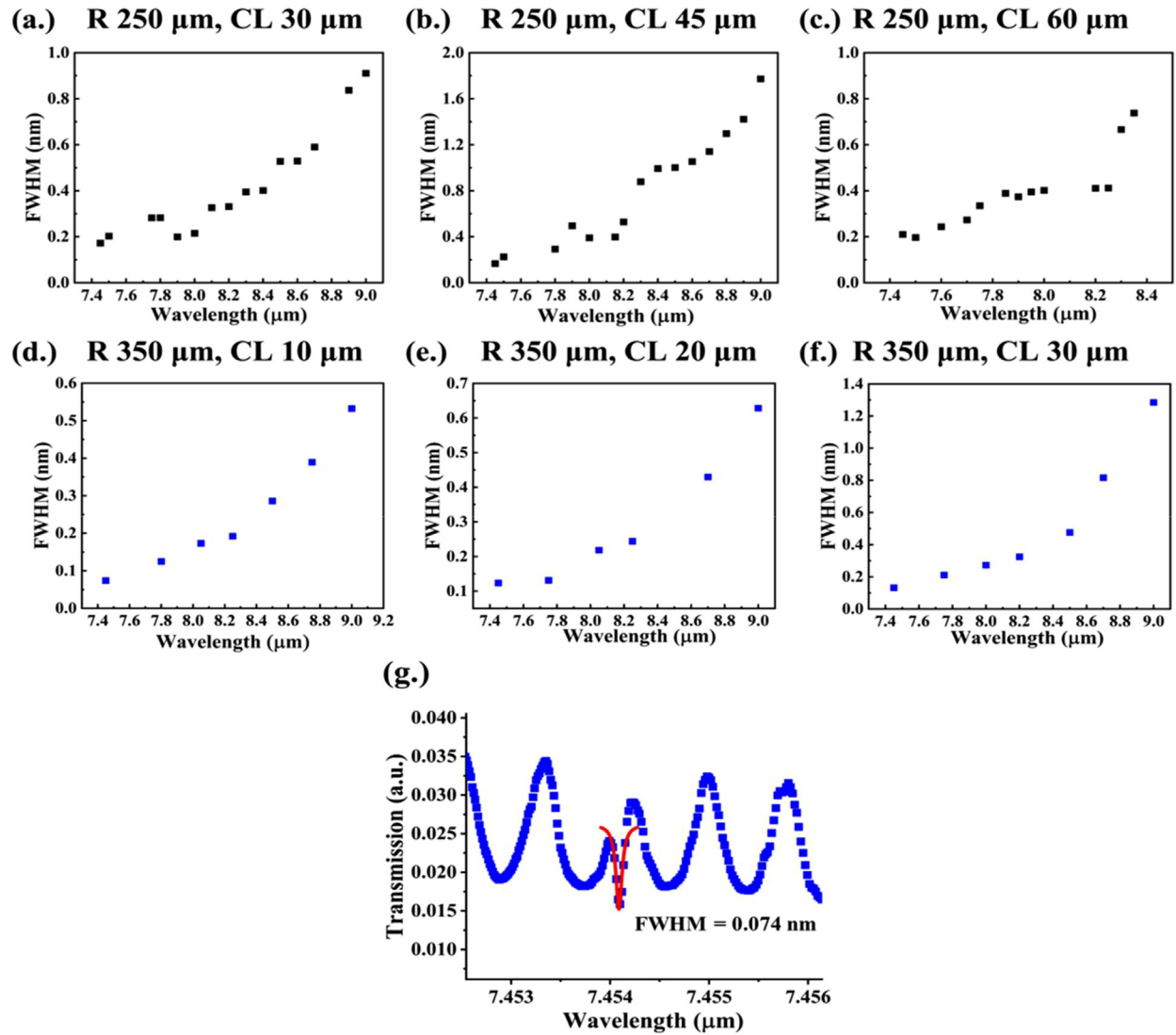
FIG. 6. Resonance FWHM as a function of the wavelength for resonator with different radius and coupling lengths (the gap is fixed at 1 μm): (a) R = 250 μm, CL = 30 μm, (b) R = 250 μm, CL = 45 μm, (c) R = 250 μm, CL = 60 μm, (d) R = 350 μm, CL = 10 μm, (e) R = 350 μm, CL = 20 μm, and (f) R = 350 μm, CL = 30 μm. (g) Example of resonator transmission as a function of the wavelength, at $\lambda = 7.45$ μm from the racetrack with the radius 350 μm and coupling length 10 μm, showing the highest Q-factor of 1.01×10^5.

bending losses as well as losses at the interface between straight waveguide and bend. To reduce the two last contributions, resonators with an increased radius of 350 μm have been fabricated and characterized. Narrower resonances have been obtained, as reported in Figs. 6(d)–6(f). The smallest value has been obtained for the coupling length of 10 μm, with a FWHM of 0.074 nm at 7.45 μm wavelength [Fig. 6(g)], which corresponds to a loaded Q-factor of 1.01×10^5. By considering this loaded Q-factor and the transmission at resonance, it is possible to deduce the intrinsic Q-factor.[9] A value of 1.13×10^5 is deduced, corresponding to total propagation losses of 1.2 dB/cm inside the resonator, which is consistent with previous measurements on graded SiGe photonic waveguides. However, again, the FWHM increases rapidly with the wavelength at a rate that is not compatible

with the variation of the coupling coefficient. At 9 μm wavelength, a loaded Q-factor of 1.70×10^4 is obtained, which corresponds to an intrinsic Q-factor of 2.03×10^4. The corresponding propagation loss is, thus, 5.6 dB/cm, which is higher than the typically 3 dB/cm propagation loss that was measured previously at 9 μm wavelength on this waveguide platform. It is believed that the difference comes from bend losses and losses at the interface between bends and straight waveguide.

In conclusion, broadband-integrated racetrack resonators have been demonstrated in the LWIR, operating from 7.45 to 9 μm wavelength. Q-factor up to 10^5 has been demonstrated. Thermal tuning of the phase in the micro-ring has been used to overcome instrumental limitations of the setup in terms of spectral resolution. These results

pave the way for the development of advanced photonics circuits in the LWIR spectral range for a wide range of applications, including sensing, spectroscopy, and communications.

AUTHOR DECLARATIONS
Conflict of Interest

The authors have no conflicts to disclose.

Author Contributions

Natnicha Koompai: Conceptualization (equal); Investigation (equal); Methodology (equal); Writing – original draft (equal); Writing – review & editing (equal). **Jean-René Coudevylle:** Methodology (equal). **David Bouville:** Methodology (equal). **Carlos Ramos:** Investigation (equal); Methodology (equal). **Laurent Vivien:** Investigation (equal); Methodology (equal). **Giovanni Isella:** Investigation (equal); Methodology (equal); Writing – review & editing (equal). **Delphine Marris-Morini:** Conceptualization (equal); Investigation (equal); Methodology (equal); Writing – review & editing (equal). **Thi Hao Nhi Nguyen:** Investigation (equal); Writing – review & editing (equal). **Victor Turpaud:** Investigation (equal). **Jacopo Frigerio:** Investigation (equal); Writing – review & editing (equal). **Virginia Falcone:** Investigation (equal). **Stefano Calcaterra:** Investigation (equal). **Luca Lucia:** Investigation (equal). **Adel Bousseksou:** Investigation (equal); Methodology (equal); Writing – review & editing (equal). **Raffaele Colombelli:** Investigation (equal); Methodology (equal); Writing – review & editing (equal).

DATA AVAILABILITY

The data that support the findings of this study are available from the corresponding author upon reasonable request.

REFERENCES

[1]H. Lin, Z. Luo, T. Gu, L. C. Kimerling, K. Wada, A. Agarwal, and J. Hu, Nanophotonics **7**(2), 393–420 (2017).
[2]L. Tombez, E. J. Zhang, J. S. Orcutt, S. Kamlapurkar, and W. M. J. Green, Optica **4**(11), 1322–1325 (2017).
[3]J. F. Dean, J. J. Middelburg, T. Röckmann, R. Aerts, L. G. Blauw, M. Egger, M. S. M. Jetten, A. E. E. de Jong, O. H. Meisel, O. Rasigraf, C. P. Slomp, M. H. in't Zandt, and A. J. Dolman, Rev. Geophys. **56**(1), 207–250, https://doi.org/10.1002/2017RG000559 (2018).
[4]V. Mittal, G. Devitt, M. Nedeljkovic, L. G. Carpenter, H. M. H. Chong, J. S. Wilkinson, S. Mahajan, and G. Z. Mashanovich, Biomed. Opt. Express **11**(8), 4714–4722 (2020).
[5]N. L. Kazanskiy, S. N. Khonina, and M. A. Butt, Photonics **9**(5), 331 (2022).
[6]F. Keilmann, C. Gohle, and R. Holzwarth, Opt. Lett. **29**(13), 1542–1544 (2004).
[7]See https://irsweep.com/ for commercially available dual-comb spectroscopic systems.
[8]M. Yu, Y. Okawachi, A. G. Griffith, N. Picqué, M. Lipson, and A. L. Gaeta, Nat. Commun. **9**(1), 1869 (2018).
[9]K. Zhang, G. Böhm, and M. A. Belkinar, Appl. Phys. Lett. **120**(6), 061106 (2022).
[10]B. Gholipour, S. R. Elliott, M. J. Müller, M. Wuttig, D. W. Hewak, B. E. Hayden, Y. Li, S. S. Jo, R. Jaramillo, R. E. Simpson, J. Tominaga, Y. Cui, A. Mandal, B. J. Eggleton, M. Rochette, M. Rezaei, I. Alamgir, H. M. Shamim, R. Kormokar, A. Anjum, G. T. Zeweldi, T. S. Karnik, J. Hu, S. O. Kasap, G. Belev, and A. Reznik, J. Phys. Photonics **5**(1), 012501 (2023).
[11]D. Thomson, A. Zilkie, J. E. Bowers, T. Komljenovic, G. T. Reed, L. Vivien, D. Marris-Morini, E. Cassan, L. Virot, J.-M. Fédéli, J.-M. Hartmann, J. H. Schmid, D.-X. Xu, F. Boeuf, P. O'Brien, G. Z. Mashanovich, and M. Nedeljkovic, J. Opt. **18**(7), 073003 (2016).
[12]R. Soref, Nat. Photonics **4**(8), 495–497 (2010).
[13]D. Marris-Morini, V. Vakarin, J. M. Ramirez, Q. Liu, A. Ballabio, J. Frigerio, M. Montesinos, C. Alonso-Ramos, X. L. Roux, S. Serna, D. Benedikovic, D. Chrastina, L. Vivien, and G. Isella, Nanophotonics **7**(11), 1781–1793 (2018).
[14]N. K. Hon, R. Soref, and B. Jalali, J. Appl. Phys. **110**(1), 011301 (2011).
[15]M. Sinobad, C. Monat, B. Luther-davies, P. Ma, S. Madden, D. J. Moss, A. Mitchell, D. Allioux, R. Orobtchouk, S. Boutami, J.-M. Hartmann, J.-M. Fedeli, and C. Grillet, Optica **5**(4), 360–366 (2018).
[16]M. Montesinos-Ballester, C. Lafforgue, J. Frigerio, A. Ballabio, V. Vakarin, Q. Liu, J. M. Ramirez, X. Le Roux, D. Bouville, A. Barzaghi, C. Alonso-Ramos, L. Vivien, G. Isella, and D. Marris-Morini, ACS Photonics **7**(12), 3423–3429 (2020).
[17]T. H. Xiao, Z. Zhao, W. Zhou, C.-Y. Chang, S. Y. Set, M. Takenaka, H. K. Tsang, Z. Cheng, and K. Goda, Opt. Lett. **43**(12), 2885–2888 (2018).
[18]M. Perestjuk, R. Armand, A. D. Torre, M. Sinobad, A. Mitchell, A. Boes, J.-M. Hartmann, J.-M. Fedeli, V. Reboud, C. Monat, and C. Grillet, in *Optical Sensors and Sensing Congress 2022* (OSA, 2022).
[19]D. A. Kozak, N. F. Tyndall, M. W. Pruessner, W. S. Rabinovich, and T. H. Stievater, Opt. Express **29**(10), 15443–15451 (2021).
[20]D. Ren, C. Dong, S. J. Addamane, and D. Burghoff, Nat. Commun. **13**(1), 5727 (2022).
[21]J. M. Ramirez, Q. Liu, V. Vakarin, X. Le Roux, J. Frigerio, A. Ballabio, C. Alonso-Ramos, E. T. Simola, L. Vivien, G. Isella, and D. Marris-Morini, Opt. Lett. **44**(2), 407–410 (2019).
[22]J. M. Ramirez, Q. Liu, V. Vakarin, J. Frigerio, A. Ballabio, X. Le Roux, D. Bouville, L. Vivien, G. Isella, and D. Marris-Morini, Opt. Express **26**(2), 870–877 (2018).
[23]C. Rosenblad, H. R. Deller, A. Dommann, T. Meyer, P. Schroeter, and H. von Känel, J. Vac. Sci. Technol., A **16**(5), 2785–2790 (1998).
[24]M. Montesinos-Ballester, Q. Liu, V. Vakarin, J. M. Ramirez, C. Alonso-Ramos, X. Le Roux, J. Frigerio, A. Ballabio, E. Talamas, L. Vivien, G. Isella, and D. Marris-Morini, Sci. Rep. **9**, 14633 (2019).